https://doi.org/10.1038/s41561-019-0472-x

nature geoscience

Role of dynamic topography in sustaining the Nile River over 30 million years

Claudio Faccenna[1,2,3]*, Petar Glišović[2,4], Alessandro Forte[5], Thorsten W. Becker[2,3], Eduardo Garzanti[6], Andrea Sembroni[1] and Zohar Gvirtzman[7,8]

The Nile is the longest river on Earth and has persisted for millions of years. It has been suggested that the Nile in its present path is ~6 million years old, whereas others argue that it may have formed much earlier in geological history. Here we present geological evidence and geodynamic model results that suggest that the Nile drainage has been stable for ~30 million years. We suggest that the Nile's longevity in essentially the same path is sustained by the persistence of a stable topographic gradient, which in turn is controlled by deeper mantle processes. We propose that a large mantle convection cell beneath the Nile region has controlled topography over the last 30 million years, inducing uplift in the Ethiopian–Yemen Dome and subsidence in the Levant Sea and northern Egypt. We conclude that the drainage system of large rivers and their evolution over time can be sustained by a dynamic topographic gradient.

The drainage systems of major rivers and their evolution over time represent fundamental, yet poorly understood, problems in geomorphology and hydrology[1–4]. This is because the laws that govern landscape evolution and the landscape's response to tectonics and climate are still poorly known. Among transcontinental drainage systems, many rivers are sourced from orogenic belts and high plateaux (for example, the Amazon, Tigris–Euphrates, Ganga–Brahmaputra and Yangtze). Others, including the Nile, the Orange and the Yenisei, flow instead from intraplate swells generated by plume-related upwellings[3]. Such rivers drain large igneous provinces in their upper reaches and are thus characterized by basaltic detritus with distinct petrographic, mineralogical and geochemical signatures[5]. The origins of some of these long-lived rivers have been discussed and, for the Amazon River[6] and rivers of Australia[7–9] and Africa[9,10], a link between dynamic topography, uplift history and river profiles has been explored.

Here, we propose that the drainage of one of the longest rivers on Earth, the Nile, is indeed controlled by topography related to mantle dynamics (that is, dynamic topography). The Nile flows for more than 6,800 km; it crosses the largest desert on Earth, and it served as a cradle of civilization in the Stone Age (Fig. 1). The Blue Nile and Atbara branches start on the volcanic Ethiopian Plateau and join into the White Nile before discharging into the Mediterranean Sea, where a large delta is present. The Nile cuts through a topographic swell forming six cataracts and has a gentle gradient in its lowest portion.

Long-running debates about the birth and life of the Nile have focused on the question of whether the present-day Nile represents the evolution of the proto-Nile that has flowed from the Ethiopian highlands since the early Tertiary period. Two competing models have been proposed: the first envisions a long-term river discharge from Ethiopia since the Oligocene epoch (~30 million years ago (Ma)) (refs. [11–15]); the second suggests that the Mediterranean was connected with Ethiopia only in the late Miocene epoch after the Messinian salinity crisis (~5.8 Ma) (refs. [16–19]), and that at earlier times detritus at the delta was derived only locally, from the western margin of the Red Sea (Red Sea Hills)[19]. In equatorial Africa, the fluvial network was believed to be directed westward as part of a palaeo-Congo continental-scale drainage system until the late Miocene onset of the East African Rift (~11–5 Ma), when river flow was diverted northward[20]. In this context, the uplift of Ethiopia would be a recent feature[21].

Here, we present geological and geophysical arguments supporting the idea that the Nile has been sustained by a mantle 'conveyor belt' operating through most of the Tertiary, with a convective upwelling centred under the Ethiopian highlands and a downwelling under the eastern Mediterranean, creating a topographic gradient that supported the Nile's course over ~30 Myr. Such a course, which is similar to the present-day one, was likely established in the early Oligocene (~30 Ma). Before that, our modelling shows that the drainage pattern was probably directed northwestward and controlled by the rifting process occurring in the Gulf of Sirte.

Source-to-sink geological evidence

As Herodotus inferred in the fifth century BC[22], Nile sediments chiefly derive from the Ethiopian highlands. Before the closure of the Aswan High Dam in 1964, the Nile Delta was receiving $230 \pm 20 \times 10^6$ tons yr^{-1} of sediment, ~95% of which derived from Ethiopian highlands tributaries (Blue Nile, $140 \pm 20 \times 10^6$ tons yr^{-1}, and Atbara, $82 \pm 10 \times 10^6$ tons yr^{-1}) (refs. [5,23]). Extrapolating the present-day sediment flux to the past is not straightforward[2,24]. For example, the dramatic sea-level fall during the Messinian salinity crisis (~5.8 Ma) produced canyons along the course of the early 'Eonile' incised to a depth of ~1.5 km under Cairo and ~170 m below the present sea level at Aswan[25].

Sediment analysis from Nile Delta cores documents the connection from the Ethiopian highlands to the Nile Delta extending back to the Oligocene[26]. Those sediments include the occurrence of

[1]Laboratory of Experimental Tectonics, Department of Sciences, Roma Tre University, Rome, Italy. [2]Department of Geological Sciences, Jackson School of Geosciences, The University of Texas at Austin, Austin, TX, USA. [3]Institute for Geophysics, Jackson School of Geosciences, The University of Texas at Austin, Austin, TX, USA. [4]Geotop, Université du Québec à Montréal, Montréal, Quebec, Canada. [5]Department of Geological Sciences, University of Florida, Gainesville, FL, USA. [6]Department of Earth and Environmental Sciences, Università di Milano-Bicocca Milano, Milan, Italy. [7]Geological Survey of Israel, Jerusalem, Israel. [8]The Hebrew University of Jerusalem, Jerusalem, Israel. *e-mail: faccenna@uniroma3.it

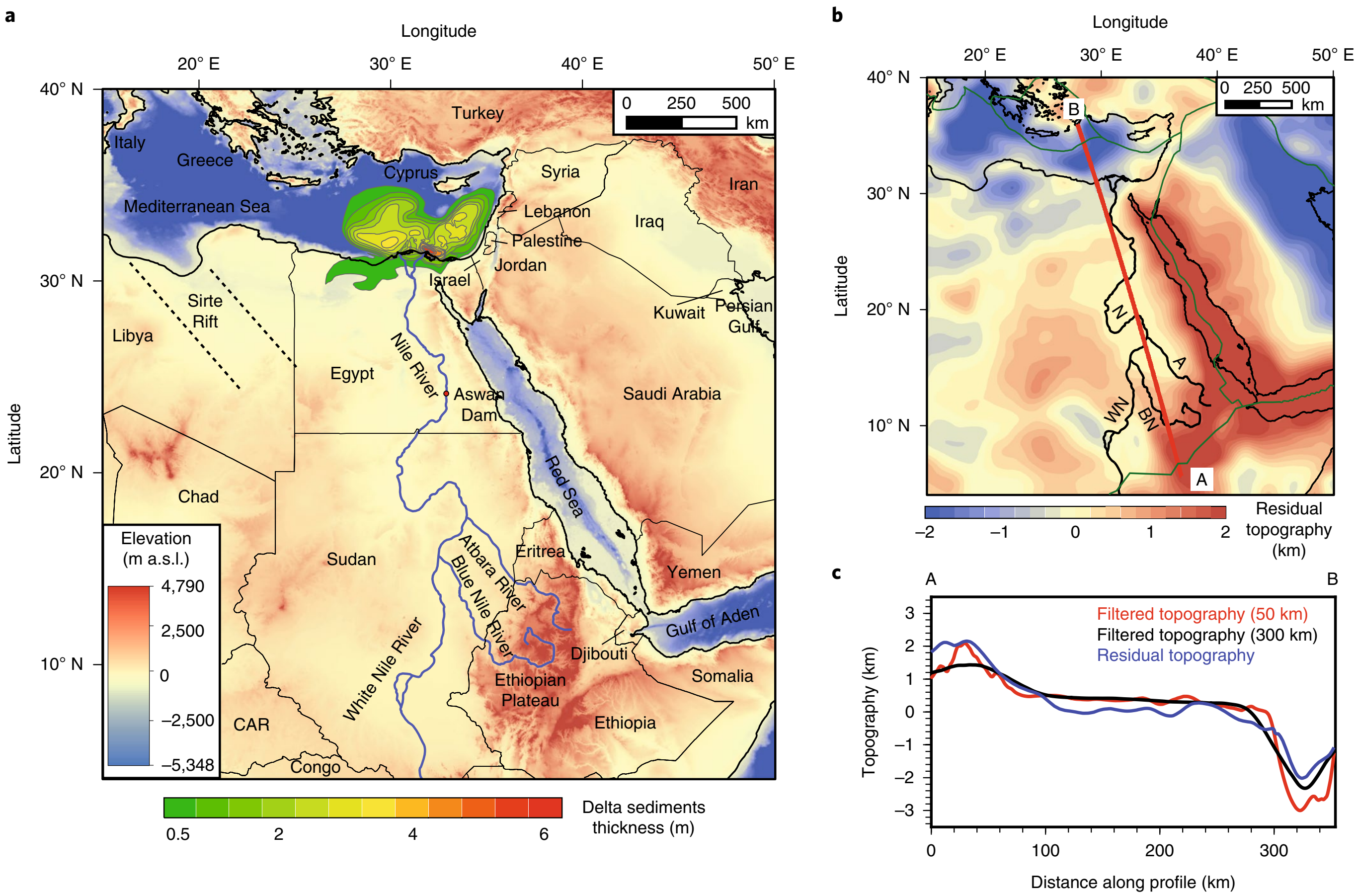

Fig. 1 | The East Africa–eastern Mediterranean sediment transport system. **a**, Topography of the Nile drainage showing thickness of upper Tertiary sediments in the Nile Delta basins including the Levantine basin (eastern lobe) and Herodotus basin (western lobe) (data from ref. [27]). Elevation in m above sea level (a.s.l.). CAR, Central African Republic. **b**, Residual topography map estimated considering crustal thickness and variable crustal density from crustal model CRUST1.0 (refs. [38,47]). River labels are WN, White Nile; BN, Blue Nile; N, Nile; and A, Atbara River. Points A and B indicate start and end points for river profile graphed in **c**. **c**, Comparison between topography and its residual component along a profile approximately following the Nile (topography is filtered in frequency domain by 50 and 300 km low pass filters).

detrital zircons yielding young uranium–lead ages (30–20 Ma), reflecting the detrital trace of bimodal Ethiopian volcanic products since the Rupelian age (~31 Ma) (ref. [26]).

An Oligocene age of the East African–Mediterranean transport system is also supported by sediment thickness data[27,28]. Figure 2 shows the total volume of fully compacted sediment in the Herodotus and Levant basins, which is estimated to be ~580,000 km^3, of which more than 30% was deposited after the Messinian age (~390,000 km^3 in the Oligocene–Miocene and 190,000 km^3 in the Pliocene–Pleistocene)[27,28]. The volume increase may in part be only an apparent increase[29], or it may be related to the gain of drainage area by river capture[30,31].

The total volume of sediment may be compared with the total amount of eroded material. This has been defined by subtracting the plateau surface (top of the flood basalt) from the present-day topography over the Ethiopian–Yemen Plateau[32]. Our best estimate is ~216,000 km^3 of eroded material over a region of 400,000 km^2, from which 33,515 km^3 (16%) are basement sedimentary or metamorphic rocks and the rest is basalt. This value is two to four times larger than previous estimates[12,27]. Although reduced by our estimate, the mismatch between eroded volumes from Ethiopia and sediment volumes deposited in the Nile Delta system remains significant, suggesting additional supply from non-Ethiopian sources in the past (including wind-blown Saharan sand and possibly sand from the White Nile and detritus from the Red Sea Hills).

Thermochronology indicates that erosion and exhumation in the Blue Nile basement units started as early as ~28–30 Ma (ref. [33]). Local estimates of the incision rate along the Blue Nile indicate three pulses of uplift since ~10 Ma (ref. [21]). However, systematic river analyses indicate an early doming episode (Oligocene) maintained for a long time[30]. The incisional history of the Blue Nile and Tekeze rivers evidences three base level changes superimposed on the uplifting bulge: the oldest one, between 20 and 10 Ma, related to capture of plateau internal drainage; the second one, between 10 and 5 Ma, related to a local tectonic event; and the last one, in the Quaternary period, related to a climatic and/or tectonic event[30].

Inversion of river profiles has been used to infer uplift rate and hence continental-scale landscape evolution over Africa, indicating a main phase of uplift starting at ~30 Ma (refs. [9,10]). However, the Nile River suffered recent reorganizations, such as the recent integration of the White Nile and of the internally drained Ethiopian Plateau[30,31] and the dramatic Messinian sea-level drop. Independently of the tectonic uplift of the Ethiopian Plateau, those processes likely modified the river profile and sedimentation rate.

We constrained our analysis of the evolution of the Ethiopian–Yemen highlands using the flood basalt as a reference layer (details in ref. [32]), reconstructing the elevation over two time periods, before and after flood basalt emplacement, that is, from about 40 to 30 Ma and from about 30 to 15 Ma, respectively (Supplementary Fig. 1). The result of this analysis shows that the Ethiopian highlands were already at an average elevation of ~750 m before the main phase of flood basalt outpouring (Fig. 2 and Supplementary Fig. 1c), increasing to ~1,250 m just after the flood basalt emplacement, at ~30 Ma (Fig. 2). After that, a large-scale doming took place, providing an average elevation of ~2,600 m (Fig. 2 and Supplementary Fig. 1b), decreasing during the rifting stage (<11 Ma) to ~2,250 m and reaching an average present-day average elevation of ~1,800 m (Fig. 2 and Supplementary Fig. 1a).

This reconstruction indicates a long-term increase in elevation of the Ethiopian Plateau, favouring more erosion and discharge over a longer time period than previously thought.

Upwelling and downwelling geophysical evidence

The Nile drains water from Lake Victoria in Uganda and partly from Lake Tana, on the Ethiopian Plateau. Several models suggest that the plateau topography is dynamically related to the upwelling of the East African, or Afar, plume[34–37]. Residual topography, that is topography relative to the inferred lithospheric isostatic contribution, shows a positive anomaly on the Ethiopian highlands of more than ~600 m (30% of the present-day elevation) (Supplementary Fig. 2). The positive residual topography is also pronounced along the Red Sea and Gulf of Aden. These patterns are stable irrespective of parameters such as crustal and lithosphere mantle density, which mainly modulate amplitude (Supplementary Fig. 2). The positive residual topography signal in the Ethiopian region is complemented by negative residual topography over northern Egypt and the Herodotus Basin (Fig. 1b). The origin of the deep bathymetry of the Herodotus–Ionian Basin (up to 4,000 m below sea level) is unclear (any flexural component due to the Hellenic slab should be significant only close to the trench[38]) and incomplete knowledge of the ocean crust thickness there prevents a precise estimate of the residual topography.

Residual topography estimates may be compared with dynamic topography, that is, the transient topography signal related to mantle convection that can be computed from tomography-based flow models (compare Figs. 1b and 3a). The present-day estimates show a remarkable positive anomaly beneath the Ethiopian–Yemen Dome extending northward beneath the Red Sea (Fig. 1b). Dynamic topography is negative within the Ionian–eastern Mediterranean Basin, extending to northern Egypt (Fig. 3a); this is similar to what is observed for residual topography (Fig. 1b).

To understand the dynamic origin and temporal evolution of Nile basin topography, we reconstruct the evolution of mantle convection beneath the African Plate through the Cenozoic era and link it to the surface geological record using an iterative data-assimilation method for time-reversed, tomography-based convection[39,40].

Figure 3c shows estimates of the dynamic configuration back to 40 Ma, before the flood-basalt outpouring and Nile Delta deposition. The reconstruction shows a low-amplitude swell in Ethiopia. Small dynamic topography is predicted in the Nile Delta region, but a negative signal is suggested in northern Sudan. This topographic configuration should not have favoured drainage from Ethiopia to Egypt. This indicates that at that time, rivers that drained into the Mediterranean Sea flowed farther to the west, possibly along the Sirte Rift that runs from northwest to southeast, which at that time was actively subsiding and being filled with a thick pile of sediments[41], indicating the activity of a large continental drainage[5,27,28] (Fig. 3f). In terms of topography, this tectonic forcing produced an additional negative tectonic signal on top of the mantle-induced dynamic component. Despite this favourable scenario, we cannot discard the possibility of an older pre-Oligocene Atlantic drainage, even though large deltas in the Atlantic did not appear before the Oligocene[5,27].

Figure 3d–f shows the predicted incremental changes of dynamic topography in 20 Myr time windows and allows an assessment of the expected landscape evolution over time considering tectonic activity confined to the Red Sea region and the Gulf of Sirte region.

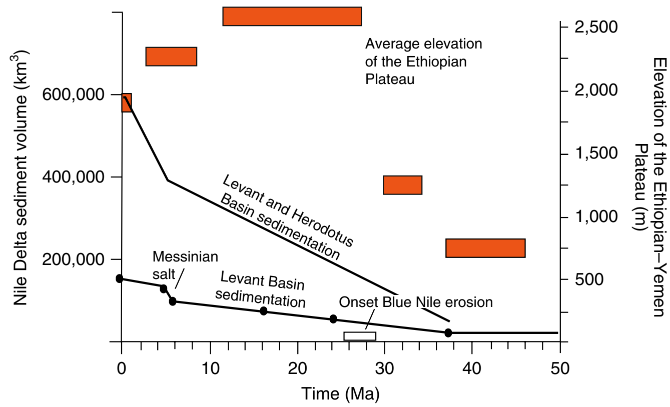

Fig. 2 | Evolution of the Ethiopian–Yemen Plateau topography (source) compared with the Nile Delta sedimentation volume (sink). Sediments indicate that deposition started at ~35 Ma and increased during the Neogene period (total volume from ref. [27] and Levant data from ref. [28]). Similarly, the inferred elevation of the Ethiopian–Yemen Plateau increased from the Eocene–Oligocene to the Neogene (dark orange boxes[32]). White box indicates the onset of Blue Nile incision[33]. See text for explanation.

Two centres of uplift are seen in the topography change from 60 to 40 Ma. There was modest doming (between ~200 and ~400 m of topography change) in the Levant and the northern half of the present-day Red Sea and a much stronger surface uplift (up to ~800 m of topography change) in southern Ethiopia (Fig. 3f). In the interval 40 to 20 Ma (Fig. 3e), the northernmost dome migrated and intensified to effectively uplift (by ~700 to ~800 m) the Arabian shoulder of the Red Sea Rift, whereas the centre of the main southern dome migrated to a location below Mount Kenya (~700 to ~800 m of uplift). The uplift in southern Ethiopia continued but was more modest (~200 m), and it extended northwest to Sudan where it intensified (~400 m). A new centre of uplift (~400 m) appeared in northern Sudan, between the present-day fifth and third cataracts of the Nile. Between 20 and 0 Ma, uplift occurred in two main regions: an elongated dome (~300 to ~400 m of uplift) encompassing Lake Tana and extending northwestward along the Blue Nile and a similarly oriented dome with peak uplift (~700 to ~800 m) at Ngorongoro Crater, extending northwest to Lake Victoria. Over the past 40 Myr, the total amplitude of uplift in the region encompassing the southern portions of the White Nile in Uganda and South Sudan has been ~1,000 m, indicating that most of the present-day features result from a continuous growth driven by the long-lived upwelling of the East African plume. This inference is in agreement with geological evidence for the East African Rift Dome, where a large-scale bulge may have formed at least in the late Eocene epoch[36,37,42] (Fig. 2). Before the outpouring of the flood basalts, at ~30 Ma, in fact, the elevation of the Ethiopian Plateau was inferred to be already ~700–800 m high on average[32] (Fig. 2 and Supplementary Fig. 1), which is partially supported by the mantle dynamic predictions (Fig. 3f).

Our reconstruction of the dynamic topography beneath the dome (that is, the Ethiopian part) indicates that the onset of uplift may have started at ~40 Ma (Fig. 4). The extent of the doming may have been large, as a large-scale, latest Eocene–early Oligocene erosional surface has been documented over northern Egypt and the Middle East[4,42,43]. This feature has been also confirmed by inversion of river profiles over similar domes formed in North Africa (Hoggar and Tibesti domes)[9,10]. We also notice a positive anomaly extending onto the Red Sea shoulder of the Arabian plate. Thermochronology data indicate a peak of erosion and uplift of the Red Sea shoulder around 20 Ma (ref. [27]) which is well in agreement with our model (Fig. 3e). This positive topographic feature, arising from a combination of tectonic and dynamic topography, provided a source of

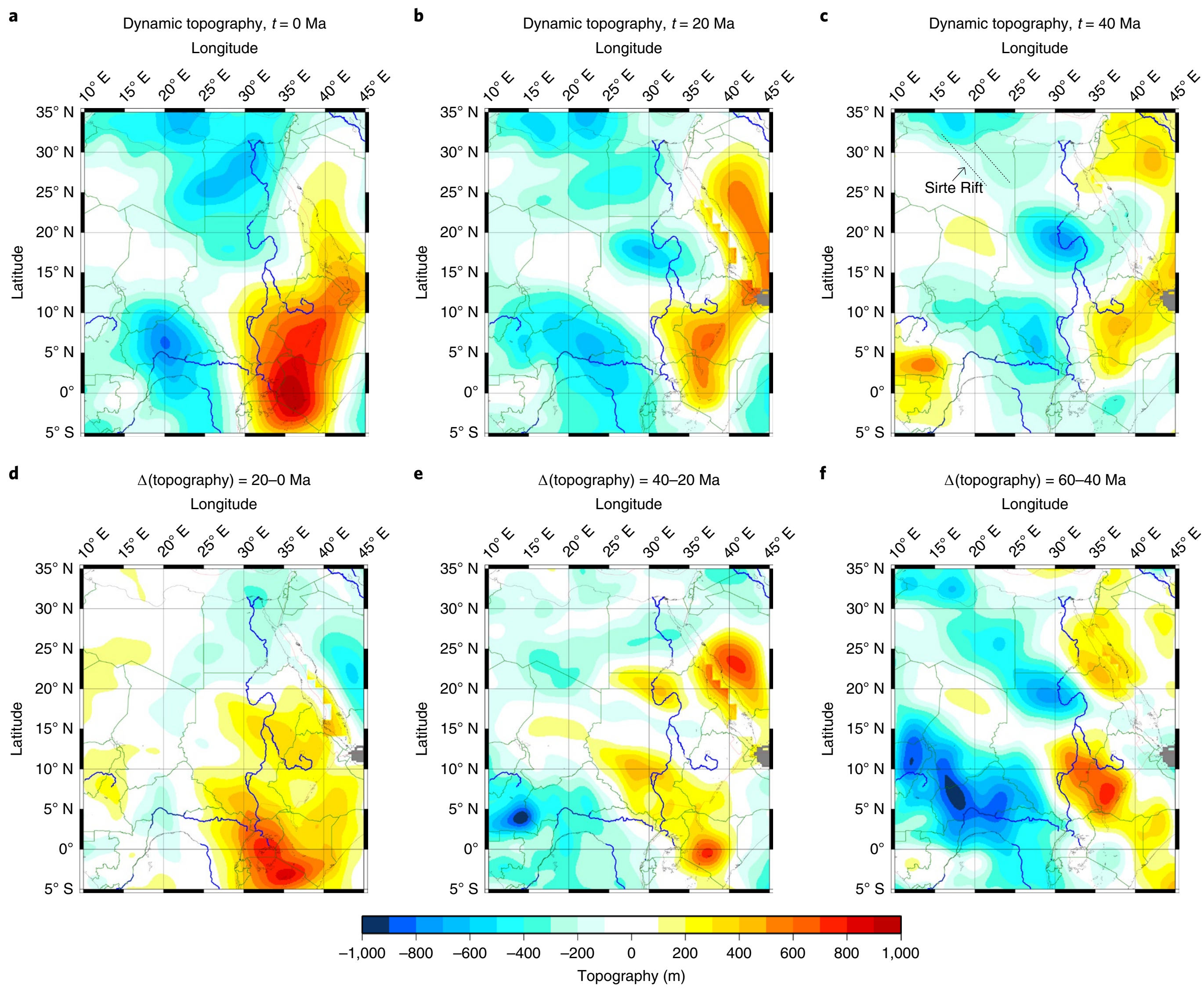

Fig. 3 | Dynamic topography and topographic change of the Nile drainage over ~60 Myr. a–c, Dynamic topography at 0 Ma (**a**), 20 Ma (**b**) and 40 Ma (**c**). **d–f**, Change in dynamic topography between 20 and 0 Ma (**d**), 40 and 20 Ma (**e**) and 60 Ma and 40 Ma (**f**). A Lagrangian perspective is employed, where the topography and topographic change are viewed by an observer fixed to each of the tectonic plates (African and Arabian) that occupy the region mapped here. The dynamic topography in each frame is therefore mapped in present-day geographic coordinates using the Euler poles of ref. [48] to calculate the corresponding rotations. The grey shaded Gulf of Aden region depicts oceanic crust whose age is younger than the time for which the topography is calculated. Figure drawn using the Generic Mapping Tools[49].

sediment for the Nile[27] and it represented a barrier preventing the Nile from flowing eastward into the Red Sea.

As noted above, we find an increase in the elevation of the Ethiopian Plateau following the main volcanic outburst (Fig. 3e), similar to what is seen in geological reconstructions (Fig. 2 and Supplementary Fig. 1). In particular, the increase in elevation of the Ethiopian–Yemen Dome between 40 Ma and present day (Supplementary Fig. 1a–c) shows a similar pattern to the one reconstructed from dynamic topography (Fig. 3a–c) but with a larger amplitude due to the isostatic contribution related to the emplacement of the flood basalt, to magmatic underplating and to the flexural component on the rift shoulders[32].

Another notable feature (Fig. 1b) is the negative dynamic topography anomaly over the eastern Mediterranean Sea and northern Egypt. This feature is inferred to have grown over time, migrating northward. The maximum negative peak is ~600 m, positioned just south of the present-day delta. The presence of this negative dynamic feature is related to the large-scale downwelling of the Hellenic–Tethyan slab. Seismic tomography shows that this structure extends into the lower mantle and as far as 1,500 km south of the present-day trench[44,45]. Tectonic and kinematic reconstructions indicate that penetration of the slab into the lower mantle occurred at ~50 ± 10 Ma (refs. [35,41,45]). Since then, the slab's progressive sinking may have favoured larger-scale subsidence. Our model (Fig. 4) predicts continuous subsidence since ~35 Ma, accelerating at ~5 Ma. This progressive subsidence appears recorded in the sedimentation rate, which increased over time and accelerated after the Messinian salinity crisis (~5.8 Ma), with a southward shift of the depocentre. Another negative dynamic topography feature extends to the Sudan–Congo Basin region and has been interpreted as return flow of the main Ethiopian plume[34].

Our model also shows small-scale, positive dynamic topography around 20° N in northern Sudan. Here, the course of the Nile describes a contorted path in a great bend which cuts through

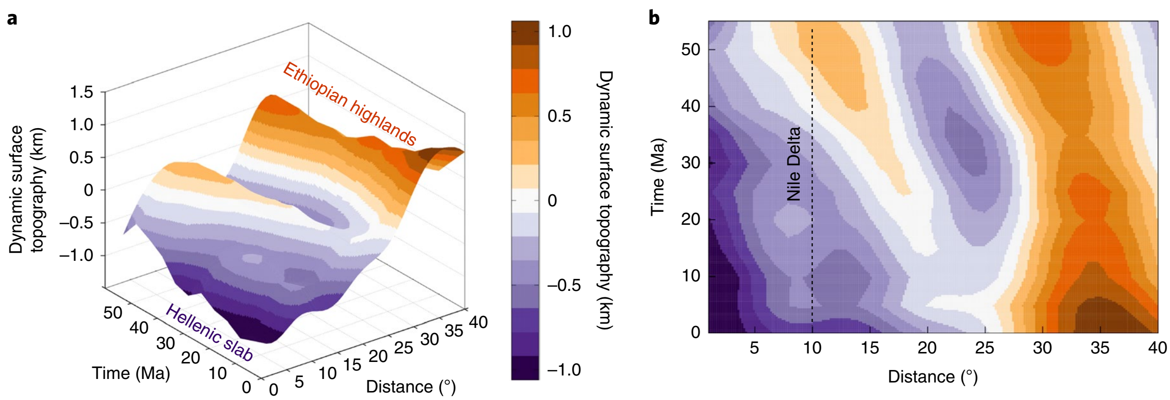

Fig. 4 | Changes in dynamic surface topography of a Nile Basin transect over 55 Myr. a,**b**, Dynamic surface topography as a function of time along a moving cross-section from the Ethiopian highlands to the Hellenic slab in 3D (**a**) and 2D (**b**) views. Note the inversion of dynamic topography of the Nile Delta beginning from the Oligocene.

basement bedrock and forms the well-known fifth and fourth cataracts. This bend of the Nile has been produced by the uplift (Fig. 3b,c) along an east–west axis to form the Nubian Swell[16].

Our model predicts uplift of a small-scale dome exactly in the Great Bend region (Fig. 3e). This provides support for a dynamic origin of the Nubian Swell[16], and further suggests that the swell may have started to form earlier, in agreement with geological data[46]. We find that small-scale positive changes in dynamic topography, such as surface uplift, occur on sites of negative dynamic topography (Fig. 3b,c,e). This negative signal is related to a small-scale return flow from the Ethiopian plume that weakened over time, therefore leading to uplift (Supplementary Fig. 4).

We infer that our topography predictions are directly reflected in river drainage but further tests are necessary to make more accurate reconstructions that include landscape evolution, crustal tectonics and climate change. However, the regional application of landscape evolution models is here complicated by the change in climate and sea level in the Mediterranean, notably during the Messinian salinity crisis, and by river and plateau area drainage capture. These processes likely modified the landscape and river incision over most of region. Nonetheless, our geodynamic model captures first-order processes and is supported by a range of geological evidence. This indicates that the Nile may have drained along a similar path since the Oligocene. Despite the multiple small-scale modifications that the Nile drainage must have undergone during the last 30 Myr, the river has existed without interruption, continuously connecting the Ethiopian topographic swell to the Mediterranean Sea. This pathway appears to have been sustained by a mantle convection cell produced by an upwelling in Ethiopia and a downwelling close to the Egypt–Levant Basin established ~40 Ma, and it is still active today (Supplementary Fig. 4). This 'conveyor belt' appears associated with a topographic gradient with an overall peak-to-trough difference of ~1.5 km, forcing the long-term drainage pattern of the Nile River to cut through other, smaller-scale dynamic topography features (for example, the Nubian Swell). This supports the idea that long-lived intra-continental rivers[6–9] and their changes over time may provide a first-order indication of dynamic topography variations and how mantle convection shapes the surface of the Earth over tens of millions of years.

Online content

Any methods, additional references, Nature Research reporting summaries, source data, statements of code and data availability and associated accession codes are available at https://doi.org/10.1038/s41561-019-0472-x.

Received: 17 August 2018; Accepted: 13 September 2019; Published online: 11 November 2019

References

1. Audley-Charles, M. G., Curray, J. R. & Evans, G. Location of major deltas. *Geology* **5**, 341–344 (1977).
2. Potter, P. E. Significance and origin of big rivers. *J. Geol.* **86**, 13–33 (1978).
3. Cox, K. G. The role of mantle plumes in the development of continental drainage patterns. *Nature* **342**, 873–877 (1989).
4. Goudie, A. S. The drainage of Africa since the Cretaceous. *Geomorphology* **67**, 437–456 (2005).
5. Garzanti, E., Andò, S., Vezzoli, G., Megid, A. A. A. & El Kammar, A. Petrology of Nile River sands (Ethiopia and Sudan): sediment budgets and erosion patterns. *Earth Planet. Sci. Lett.* **252**, 327–341 (2006).
6. Shephard, G. E., Müller, R. D., Liu, L. & Gurnis, M. Miocene drainage reversal of the Amazon River driven by plate–mantle interaction. *Nat. Geosci.* **3**, 870–875 (2010).
7. Salles, T., Flament, N. & Müller, D. Influence of mantle flow on the drainage of eastern Australia since the Jurassic Period. *Geochem. Geophys. Geosyst.* **18**, 280–305 (2017).
8. Czarnota, K., Roberts, G. G., White, N. J. & Fishwick, S. Spatial and temporal patterns of Australian dynamic topography from River Profile Modeling. *J. Geophys. Res. Solid Earth* **119**, 1384–1424 (2014).
9. Rudge, J. F., Roberts, G. G., White, N. J. & Richardson, C. N. Uplift histories of Africa and Australia from linear inverse modeling of drainage inventories. *J. Geophys. Res. Earth* **120**, 894–914 (2015).
10. Paul, J. D., Roberts, G. G. & White, N. The African landscape through space and time. *Tectonics* **33**, 898–935 (2014).
11. McDougall, I., Morton, W. H. & Williams, M. A. J. Age and rates of denudation of Trap Series basalts at Blue Nile Gorge, Ethiopia. *Nature* **254**, 207–209 (1975).
12. Williams, M. A. J. & Williams, F. M. in *The Sahara and the Nile* (eds Williams, M. A. J. & Faure, H.) 207–224 (A. A. Balkema, 1980).
13. Burke, K. & Wells, G. L. Trans-African drainage system of the Sahara: was it the Nile? *Geology* **17**, 743–747 (1989).
14. Pik, R., Marty, B., Carignan, J. & Lavé, J. Stability of the Upper Nile drainage network (Ethiopia) deduced from (U–Th)/He thermochronometry: implications for uplift and erosion of the Afar plume dome. *Earth Planet. Sci. Lett.* **215**, 73–88 (2003).
15. Abdelkareem, M., Ghoneim, E., El-Baz, F. & Askalany, M. New insight on paleoriver development in the Nile basin of the eastern Sahara. *J. Afr. Earth Sci.* **62**, 35–40 (2012).
16. Stern, R. J. & Abdelsalam, M. G. The origin of the great bend of the Nile from SIR-C/X-SAR imagery. *Science* **274**, 1696–1698 (1996).
17. Butzer, K. W. & Hansen, C. L. *Desert and River in Nubia* (Univ. Wisconsin Press, 1968).
18. Said, R. *The River Nile: Geology, Hydrology and Utilization* (Elsevier, 1993).
19. Issawi, B. & McCauley, J. F. in *The Followers of Horus, Studies Dedicated to Michael Allen Hoffman 1944–1990* (eds Friedman, R. F. & Adams, B.) 121–138 (Oxford Univ. Press, 1992).
20. Talbot, M. R. & Williams, M. A. J. in *The Nile—Origin, Environments, Limnology and Human Use* (ed. Dumont, H. J.) 37–70 (Springer, 2009).

21. Gani, N. D., Abdelsalam, M. G. & Gani, M. R. Blue Nile incision on the Ethiopian Plateau: pulsed plateau growth, Pliocene uplift, and hominin evolution. *Geol. Soc. Am. Today* **17**, 4–11 (2007).
22. Wainwright, G. A. Herodotus II, 28 on the sources of the Nile. *J. Hellenic Stud.* **73**, 104–107 (1953).
23. Padoan, M., Garzanti, E., Harlavan, Y. & Villa, I. M. Tracing Nile sediment sources by Sr and Nd isotope signatures (Uganda, Ethiopia, Sudan). *Geochim. Cosmochim. Acta* **75**, 3627–3644 (2011).
24. Garzanti, E., Andò, S., Padoan, M., Vezzoli, G. & El Kammar, A. The modern Nile sediment system: processes and products. *Quat. Sci. Rev.* **130**, 9–56 (2015).
25. Chumakov, I. S. in *Desert and River in Nubia: Geomorphology and Prehistoric Environments at the Aswan Reservoir* (eds Butzer, K. A. & Hansen, C. L.) 521–522 (Univ. Wisconsin Press, 1968).
26. Fielding, L. et al. The initiation and evolution of the River Nile. *Earth Planet. Sci. Lett.* **489**, 166–178 (2018).
27. Macgregor, D. S. The development of the Nile drainage system: integration of onshore and offshore evidence. *Petrol. Geosci.* **18**, 417–431 (2012).
28. Steinberg, J., Gvirtzman, Z., Folkman, Y. & Garfunkel, Z. Origin and nature of the Tertiary infilling of the Levant Basin. *Geology* **39**, 355–358 (2011).
29. Schumer, R. & Jerolmack, D. J. Real and apparent changes in sediment deposition rates through time. *J. Geophys. Res. Earth.* **114**, F00A06 (2009).
30. Sembroni, A., Molin, P., Pazzaglia, F. J., Faccenna, C. & Bekele, A. Evolution of continental-scale drainage in response to mantle dynamics and surface processes: an example from the Ethiopian Highlands. *Geomorphology* **261**, 12–29 (2016).
31. Giachetta, E. & Willett, S. D. Effects of river capture and sediment flux on the evolution of plateaus: insights from numerical modeling and river profile analysis in the upper Blue Nile catchment. *J. Geophy. Res. Earth* **123**, 1187–1217 (2018).
32. Sembroni, A., Faccenna, C., Becker, T. W., Molin, P. & Bekele, A. Long-term, deep mantle support of the Ethiopia-Yemen Plateau. *Tectonics* **35**, 469–488 (2016).
33. Pik, R., Marty, B., Carignan, J., Yirgu, G. & Ayalew, T. Timing of East African Rift development in southern Ethiopia: implication for mantle plume activity and evolution of topography. *Geology* **36**, 167–170 (2008).
34. Moucha, R. & Forte, A. M. Changes in African topography driven by mantle convection. *Nat. Geosci.* **4**, 707–712 (2011).
35. Faccenna, C., Becker, T. W., Jolivet, L. & Keskin, M. Mantle convection in the Middle East: reconciling Afar upwelling, Arabia indentation and Aegean trench rollback. *Earth Planet. Sci. Lett.* **375**, 254–269 (2013).
36. Ebinger, C. & Sleep, N. H. Cenozoic magmatism in central and east Africa resulting from impact of one large plume. *Nature* **395**, 788–791 (1998).
37. Şengör, A. M. C. in *Mantle Plumes: Their Identification through Time* Vol. 352 (eds Ernst, R. E. & Buchan, K. L.) 183–225 (Geological Society of America, 2001).
38. Gvirtzman, Z., Faccenna, C. & Becker, T. W. Isostasy, flexure, and dynamic topography. *Tectonophysics* **683**, 255–271 (2016).
39. Glišović, P. & Forte, A. M. A new back-and-forth iterative method for time-reversed convection modeling: implications for the Cenozoic evolution of 3-D structure and dynamics of the mantle. *J. Geophys. Res. Solid Earth* **121**, 4067–4084 (2016).
40. Glišović, P. & Forte, A. M. On the deep-mantle origin of the Deccan Traps. *Science* **355**, 613–616 (2017).
41. Capitanio, F. A., Faccenna, C. & Funiciello, R. The opening of Sirte basin: result of slab avalanching? *Earth Planet. Sci. Lett.* **285**, 210–216 (2009).
42. Burke, K. The African plate. *J. Afr. Earth Sci.* **99**, 341–409 (1996).
43. Avni, Y., Segev, A. & Ginat, H. Oligocene regional denudation of the northern Afar dome: pre- and syn-breakup stages of the Afro-Arabian plate. *Geol. Soc. Am. Bull.* **124**, 1871–1897 (2012).
44. Van der Voo, R., Spakman, W. & Bijwaard, H. Tethyan subducted slabs under India. *Earth Planet. Sci. Lett.* **171**, 7–20 (1999).
45. Faccenna, C., Jolivet, L., Piromallo, C. & Morelli, A. Subduction and the depth of convection in the Mediterranean mantle. *J. Geophys. Res. Solid Earth* **108**, 2099 (2003).
46. Barazi, N. & Kuss, J. Southernmost outcrops of marine lower Tertiary carbonate rocks in NE-Africa (Gebel Abyad, Sudan). *Geol. Rundschau* **76**, 529–537 (1987).
47. Laske, G., Masters, G., Ma, Z. & Pasyanos, M. Update on CRUST1.0—a 1-degree global model of Earth's crust. *EGU General Assembly Conf.* **15**, abstr. 2658 (2013).
48. Rowley, D. B. et al. Kinematics and dynamics of the East Pacific Rise linked to a stable, deep-mantle upwelling. *Sci. Adv.* **2**, e1601107 (2016).
49. Wessel, P., Smith, W. H. F., Scharroo, R., Luis, J. & Wobbe, F. Generic Mapping Tools: improved version released. *EOS Trans. AGU* **94**, 409–410 (2013).

Methods

To solve the direct (forward-in-time) problem of thermal convection in the Earth's mantle, we use the system of governing equations that satisfy conservation of mass, momentum and energy for a Newtonian viscous fluid in a compressible and self-gravitating mantle[50]. Details concerning the solution of the regularized, time-reversed energy equation are presented in ref. [51].

We carry out all flow computations using spherical harmonic expansions up to a maximum harmonic degree of 170, which yields a horizontal spatial resolution that varies from ~64 km at the core–mantle boundary to ~117 km at the top of the mantle. The vertical resolution is defined with a Chebyshev polynomial expansion up to order 129, which translates into a radial resolution length scale of from ~0.4 km near the isothermal boundaries to ~35 km in the middle of the mantle.

Two fundamental inputs for the convection models are the geodynamically constrained reference structure of the mantle and the three-dimensional (3D) buoyancy structure of the mantle derived from joint seismic–geodynamic tomography inversions.

The reference structure (viscosity, density, gravity, thermal conductivity, heat capacity and thermal expansion) is from ref. [50]. The internal (radioactive and secular cooling) energy sources are uniformly distributed through all depths and give a total of 24 TW. We opted to work with a depth-dependent viscosity profile that has been verified against a wide suite of geodynamic surface constraints[52] and independent mineral–physical modelling[53]. We also employed a purely adiabatic geotherm without (upper and bottom) thermal boundary layers. We constructed this adiabatic geotherm based on the mean temperature at the top of the upper mantle transition zone given by ref. [54], where the temperatures at the phase change horizons at 410 km and 660 km depth are 1,760 K and 1,880 K, respectively. We use isothermal conditions for both the surface and the core–mantle boundary (CMB). The surface potential temperature is 1,600 K and the CMB temperature is 2,456 K.

In our calculations of mantle flow, we employ a plate-like mechanical surface boundary condition. This boundary condition involves the viscous coupling of plate motions to the underlying mantle flow such that, at all times, the buoyancy-induced mantle flow drives the plate motions and not the inverse. The input required in the coupling of plates to mantle flow is the history of changing plate geometries during the Cenozoic, as determined from the analysis of ocean floor ages and magnetic anomalies[48]. These plate reconstructions are derived in the Indo-Atlantic hotspot reference frame, sampled across time windows of 5 Myr. Modelling the plate coupling to mantle flow is carried out in the no-net rotation reference frame. The implementation of this plate-like boundary condition involves the generation of nearly equipartitioned upper-mantle poloidal (convergent and divergent) and toroidal (strike slip) flows[55]. The compatibility between the plate reconstructions employed in our backward convection modelling[48] and another independent set of plate reconstructions are illustrated in ref. [40].

Geologically reconstructed plate velocities provide the only available, direct constraints on the past evolution of 3D buoyancy in the mantle. We therefore developed an inverse procedure that determines the smallest perturbations in the reconstructed 3D buoyancy that yield a match to the geological estimates of past plate motions at selected instants[39]. This procedure allows an objective mapping of those regions in the mantle that require a minimum 'nudge' to the reconstructed buoyancy field to match the geologically determined plate motions[39,40].

The single most important input for the mantle convection simulations is the 3D distribution of lateral temperature anomalies derived from the GyPSuM global tomography model, which simultaneously fits both seismic and geodynamic data, and mineral physical constraints on thermal contributions to 3D mantle structure[56]. To reconstruct the evolution of mantle heterogeneity, time is divided into discrete time windows bounded between a start time t_i and a finish time t_{i+1} (where time t increases positively into the past and i is the time window number)[39]. All time windows span 2.5 Myr, extending from 0 Ma to 70 Ma.

In each time window, the temperature field at the start time T_j^S is iteratively updated or modified as follows:

$$T_j^S(t_i) = \begin{cases} T_0(t_i), j = 1 \\ T_0(t_i) + W\sum_{j=2}^{n}\left[T_0(t_i) - T_{j-1}^p(t_i)\right], j \geq 2 \end{cases} \quad (1)$$

where T_0 is the initial solution at the beginning of a sequence, T_{j-1}^p is a prediction obtained by the direct (forward-in-time) integration of the preceding inverse (backward-in-time) solution at t_{i+1}, W is a 'nudging' multiplier for which the prescribed value is 0.75, and j is the iteration number. This time-sequence iteration proceeds until the variance reduction between the prediction and the initial solution converges to a minimum value at the start time (typically at $j = 5$). On the final iteration, the reconstructed temperature field at the finish time is stored and employed as the starting condition for the next time window in the past.

The geodynamic consistency of our iterative convection modelling is verified by comparing global predictions of present-day convection-related surface signals—such as tectonic plate motions, gravity anomalies and dynamic surface topography—against corresponding observations[39]. In a further check, we confirm that when they are integrated forward in time from 70 Ma to the present day, we find high global correlations to density anomalies throughout the mantle in the initial joint seismic–geodynamic topography model[39].

Dynamic topography from convection is determined by calculating flow-induced vertical stresses exerted at Earth's solid surface and balancing them against the corresponding loads associated with the undulations of the bounding surface. This load balance assumes the jump in mean density across the surface corresponds to a rock–air transition, which is appropriate for continental regions. Buoyancy forces from all mantle sources, including the lithosphere and extending down to the core–mantle boundary, are included in the calculation of surface stress. Moreover, in the modelling of flow-induced stress, the dynamic feedback of the plate-like surface boundary condition is included. The latter implies the use of mixed free-slip and no-slip surface condition[57]. Our models are global in scale and, in this work, we focus on the implications for the Nile basin (Fig. 1). A detailed review of the mathematical and physical methods employed in modelling dynamic topography is presented in ref. [57].

Data availability

Mantle and dynamic topography data analysed in this study were previously published in refs. [39,40]. Additional data related to this paper have been deposited with the Geotop Research Centre on the Dynamics of the Earth System (https://www.geotop.ca/fr/recherche/donnees/geophysique). Crustal data and residual topography data are available in Zenodo with the identifier https://doi.org/10.5281/zenodo.3405359. Data from the Levant basin were previously published[28] and are available at the website of the subsurface research lab at Geological Society of Israel (http://www.gsi.gov.il/eng/?CategoryID=239&ArticleID=598). Data on the evolution of the Ethiopian Plateau were published in ref. [32].

Code availability

Mantle-flow kernels employed to calculate mantle temperature structure and the dynamic topography predictions have been published in ref. [58] and deposited with the Geotop Research Centre on the Dynamics of the Earth System (https://www.geotop.ca/fr/recherche/donnees/geophysique). Figure 3 and Supplementary Fig. 3 were drawn using the Generic Mapping Tools (ref. [49], https://www.soest.hawaii.edu/gmt/).

References

50. Glišović, P., Forte, A. & Moucha, R. Time-dependent convection models of mantle thermal structure constrained by seismic tomography and geodynamics: implications for mantle plume dynamics and CMB heat flux. *Geophys. J. Int.* **190**, 785–815 (2012).
51. Glišović, P. & Forte, A. M. Reconstructing the Cenozoic evolution of the mantle: implications for mantle plume dynamics under the Pacific and Indian Plates. *Earth Planet. Sci. Lett.* **390**, 146–156 (2014).
52. Mitrovica, J. X. & Forte, A. M. A new inference of mantle viscosity based upon joint inversion of convection and glacial isostatic adjustment data. *Earth Planet. Sci. Lett.* **225**, 177–189 (2004).
53. Glišović, P., Forte, A. M. & Ammann, M. W. Variations in grain size and viscosity based on vacancy diffusion in minerals, seismic tomography, and geodynamically inferred mantle rheology. *Geophys. Res. Lett.* **42**, 6278–6286 (2015).
54. Katsura, T. et al. Olivine-wadsleyite transition in the system $(Mg,Fe)_2SiO_4$. *J. Geophys. Res. Solid Earth* **109**, B02209 (2004).
55. Forte, A. M. & Peltier, W. R. The kinematics and dynamics of poloidal–toroidal coupling in mantle flow: the importance of surface plates and lateral viscosity variations. *Adv. Geophys.* **36**, 1–119 (1994).
56. Simmons, N. A., Forte, A. M., Boschi, L. & Grand, S. P. GyPSuM: a joint tomographic model of mantle density and seismic wave speeds. *J. Geophys. Res. Solid Earth* **115**, B12310 (2010).
57. Forte, A. M., Simmons, N. A. & Grand, S. P. in *Treatise on Geophysics* 2nd edn (ed. Schubert, G.) 853–907 (Elsevier, 2015).
58. Glišović, P. & Forte, A. M. Two deep-mantle sources for Paleocene doming and volcanism in the North Atlantic. *Proc. Natl Acad. Sci. USA* **116**, 13227–13232 (2019).

Acknowledgements

C.F., A.S. and E.G. are supported by a MIUR Dipartimento Eccellenza grant. T.W.B. was supported by NASA OSP 201601412. P.G. and A.F. acknowledge support from the Natural Sciences and Engineering Research Council of Canada (Grant 217272-2013-RGPIN). A.F. was supported by the University of Florida. The convection simulations in this study were carried out thanks to supercomputing facilities of Calcul Québec consortia at Université de Montréal and on the HiPerGator at the University of Florida.

Author contributions

C.F. with T.W.B. conceived this study and estimated the residual and present-day dynamic topography. C.F. led writing the manuscript. P.G. and A.F. provided the mantle convection simulations and associated time-evolving dynamic topography calculations, E.G. contributed to constraints on the evolution of the Nile Basin, A.S. and C.F. on the Ethiopian highlands and Z.G. on the Levant Basin–Nile Delta evolution. All authors contributed to the writing and discussion of the science.

Competing interests

The authors declare no competing interests.

Additional information

Supplementary information is available for this paper at https://doi.org/10.1038/s41561-019-0472-x.

Correspondence and requests for materials should be addressed to C.F.

Peer review information Primary Handling Editor(s): Melissa Plail; Heike Langenberg.